Molecular Therapy
Nucleic Acids
Original Article

USP10 Targeted Self-Deliverable siRNA to Prevent Scarring in the Cornea

Edward F. Boumil,[1,5] Nileyma Castro,[1,5] Andrew T. Phillips,[1] Jon E. Chatterton,[2] Sean M. McCauley,[3] Alexey D. Wolfson,[3] Taisia Shmushkovich,[3] Marc Ridilla,[4] and Audrey M. Bernstein[1]

[1]Department of Ophthalmology and Visual Sciences, SUNY Upstate Medical University, 750 East Adams Street, Syracuse, NY 13210, USA; [2]Generation Bio, 215 First Street, Cambridge, MA 02142, USA; [3]Advirna, 60 Prescott Street, Worcester, MA 01605, USA; [4]Repair Biotechnologies, 841 East Fayette Street, Syracuse, NY 13210, USA

Ocular scarring after surgery, trauma, or infection leads to vision loss. The transparent cornea is an excellent model system to test anti-scarring therapies. Cholesterol-conjugated fully modified asymmetric small interfering RNAs (siRNAs) (self-deliverable siRNAs [sdRNAs]) are a novel modality for in vivo gene knockdown, transfecting cells and tissues without any additional formulations. Myofibroblasts are a main contributor to scarring and fibrosis. α_v integrins play a central role in myofibroblast pathological adhesion, overcontraction, and transforming growth factor β (TGF-β) activation. Previously, we demonstrated that α_v integrins are protected from intracellular degradation after wounding by upregulation of the deubiquitinase (DUB) ubiquitin-specific protease 10 (USP10), leading to integrin cell surface accumulation. In this study, we tested whether knockdown of USP10 with a USP10-targeting sdRNA (termed US09) will reduce scarring after wounding a rabbit cornea in vivo. The wounded corneal stroma was treated once with US09 or non-targeting control (NTC) sdRNA. At 6 weeks US09 treatment resulted in faster wound closure, limited scarring, and suppression of fibrotic markers and immune response. Specifically, fibronectin-extra domain A (EDA), collagen III, and a-smooth muscle actin ($p < 0.05$), $CD45^+$ cell infiltration ($p < 0.01$), and apoptosis at 24 ($p < 0.01$) and 48 h ($p < 0.05$) were reduced post-wounding. Corneal thickness and cell proliferation were restored to unwounded parameters. Targeting the DUB, USP10 is a novel strategy to reduce scarring. This study indicates that ubiquitin-mediated pathways should be considered in the pathogenesis of fibrotic healing.

INTRODUCTION

Regenerative wound healing in the eye has special importance because unlike other tissues, scarring leads to vision loss. Clinically, the global burden of ocular scarring is significant. Corneal scarring results from mechanical injury, burn, infection, or surgery.[1] Other examples of ocular scarring include glaucoma filtration surgery (the bleb to relieve intraocular pressure can heal fibrotically)[2] and other ocular morbidity such as proliferative vitreoretinopathy (PVR) and retinal detachment.[3,4] Mitomycin C (MMC) to improve healing and avert scarring is a standard of care for some of these indications, but there is a high failure rate with the filtration surgery and cell toxicity concerns in corneal surgeries.[2,5–8] Although there are several other therapeutic modalities being tested for the cornea, including viral delivery of genes, growth factors, and stem cells derived from various sources,[1,9–15] currently transplant of non-autologous corneal tissue is the only option available. Furthermore, there is a global shortage of tissue and limited access to this procedure for most of the world.[16]

As a model system, the cornea is particularly interesting for wound healing studies because it is transparent, non-transplantable human tissue is readily available, and eyes are easily accessible for microscopic analysis *in vivo*. The human cornea consists of five main layers, i.e., epithelium, Bowman's membrane, stroma, Descemet's membrane, and endothelium.[17,18] Bowman's membrane is beneath the epithelium that separates the epithelium from the stroma and is key to the healing response.[19,20] When Bowman's membrane is breached, growth factors such as transforming growth factor β (TGF-β) from the epithelium and tears reach the stroma, inducing a reaction that leads to pathological myofibroblast formation. Similarly, an intact Descemet's membrane prevents posterior fibrosis.[21] Although myofibroblasts are integral to the healing response, timed myofibroblast apoptosis or reduced development of myofibroblasts is necessary for regenerative healing.[22] The persistence of myofibroblasts in a healing wound leads to scarring.[23] Chronic fibrotic conditions in dermal, lung, liver, and kidney tissue are also characterized by myofibroblast persistence.[24–27] Thus, targeting myofibroblasts is a goal of fibrotic therapies, and the transparent cornea is an interesting and accessible model system for testing even non-ocular anti-fibrotic therapies.[20]

Our previous work on scarring has focused on the contribution of α_v integrins to myofibroblast development and persistence.[28,29] Integrins are heterodimeric transmembrane proteins that bind to the extracellular matrix (ECM) and intracellularly to the actin cytoskeleton, regulating cell adhesion, cell motility, and apoptosis. An increase in

Received 10 February 2020; accepted 22 July 2020;
https://doi.org/10.1016/j.omtn.2020.07.032.

[5]These authors contributed equally to this work.

Correspondence: Audrey Bernstein, Department of Ophthalmology and Visual Sciences, SUNY Upstate Medical University, 750 East Adams Street, Syracuse, NY 13210, USA.
E-mail: bernstea@upstate.edu

cell-surface expression of α_v-containing integrins ($\alpha_v\beta_1$, $\alpha_v\beta_3$, $\alpha_v\beta_5$, $\alpha_v\beta_6$, and $\alpha_v\beta_8$) throughout many organs promotes fibrosis,[30–32] whereas genetic silencing of α_v, and a blocking α_v peptide, prevents fibrosis in mice,[33,34] demonstrating that lowering α_v integrin levels and activity is therapeutically important. After wounding, integrins accumulate on the cell surface of myofibroblasts, increasing cell adhesion and cellular tension that promotes the expression and organization of α-smooth muscle actin (α-SMA) stress fibers that characterize myofibroblasts. Integrin engagement with the ECM also activates matrix-associated endogenous TGF-β by binding to the RGD domain in its latency-associated peptide (LAP)[30,35] and releasing TGF-β.[36,37] This active TGF-β creates an autocrine loop of TGF-β activity that results in pathological cell adhesion and secretion of fibrotic ECM such as collagen III (Col III), cellular fibronectin-extra domain A (FN-EDA), and vitronectin.[38]

We have investigated the role of α_v integrin ubiquitination in generating increased cell-surface expression on myofibroblasts during stromal healing. Integrins are ubiquitinated on the intracellular C terminus targeting them for degradation.[39] The biological effects of post-translational modifications of integrins is a burgeoning field of study. Previously, we performed RNA sequencing (RNA-seq) on pathological human primary myofibroblasts, leading to the discovery of a novel mechanism for post-wounding integrin accumulation. The protection of integrins from intracellular proteolysis shifts the balance of normal integrin homeostasis to integrin accumulation.[28] Specifically, wounding increases the expression of the deubiquitinase (DUB) USP10 (ubiquitin-specific protease 10). Mechanistically, we found that in primary human corneal myofibroblasts, USP10 removes ubiquitin from β_1 and β_5 (the α_v subunit is not ubiquitinated),[39,40] resulting in their accumulation on the cell surface and activating TGF-β.[28] Together, the augmented integrin and TGF-β activity induces myofibroblast differentiation and FN-EDA expression and organization, making USP10 a novel driver of scarring. Knockdown of USP10 with small interfering RNA (siRNA) post-translationally reduced integrin expression and prevented fibrotic marker development in an *ex vivo* pig corneal organ culture wounding model.[28,41]

USP10 is also a DUB for p53.[42] Much of the USP10-focused research has been centered on its role in cancer and the regulation of p53. Our data demonstrate that knockdown of USP10 after wounding in healthy tissue significantly reduces apoptosis and subsequent immune cell infiltration. Taken together, these data suggest that USP10 is a central regulator of integrin and apoptotic functions.

Given the accessibility of the eye, treatment of ocular disease with siRNAs is an important new modality.[43,44] To understand the different functions of USP10 in wound healing, we have performed an *in vivo* knockdown using self-deliverable RNAi technology (sdRNAi). This approach is based on the use of fully modified asymmetric siRNA conjugated to cholesterol. These cholesterol-siRNA conjugates do not require any formulation (i.e., lipids or nanoparticles) for delivery to cells and can transfect all cell types *in vitro* and *in vivo*.[45] The *in vivo* use of the self-deliverable cholesterol conjugates is especially efficient in combination with a local delivery,[46,47] as we demonstrate in the cornea. The use of the first generation of partially modified siRNA-cholesterol conjugates demonstrated efficient and prolonged knockdown efficacy in the eye.[47] Since full backbone modification of self-deliverable siRNAs (sdRNAs) significantly enhances their *in vivo* activity,[48] we created a fully modified sdRNA targeting rabbit USP10. These sdRNAs are resistant to nucleases, can be delivered to target tissues by a selection of the appropriate ligand, and demonstrate *in vivo* efficacy for months after a single treatment.[45,48] Herein, we demonstrate that a one-time dosing of sdRNA targeting USP10 in rabbits was sufficient to significantly reduce scarring after wounding at 6 weeks.

RESULTS

Identifying USP10 Targeting siRNA for *In Vivo* Rabbit Studies

Since the public RefSeq database contained only computationally-predicted rabbit USP10 sequences, we sequenced the USP10 in rabbit cornea. The resulting common "consensus" sequence for rabbit USP10 was used for the sdRNA design (see Materials and Methods; GenBank: MN927131). The USP10 targeting siRNA compound was selected from 10 lead candidates identified by an *in silico* prediction algorithm.[49] sdRNAs were produced and screened for knockdown of rabbit USP10 by qPCR. Of the 10, the sdRNA compound named US09 demonstrated the most effective knockdown in primary rabbit corneal fibroblasts (Figure 1A). Dose-response curves up to 2 μM for the best two compounds, US02 and US09, are presented in Figure S1. Figure 1B demonstrates the efficacy of cholesterol-modified non-targeting sdRNA (MAP4K4 sdRNA-Cy3) for entry into rabbit corneal fibroblasts in contrast to non-modified, non-targeting siRNA (MAP4K4 siRNA-Cy3). The general structure of sdRNA is depicted in Figure 1C. For these *in vivo* studies we have used US09 additionally modified with vinyl-phosphonate to increase the longevity of the effect.[50]

Depicted in Figure 1D is the wounding strategy. To wound the cornea, a 6-mm trephine is placed in the central rabbit cornea. A subtle twisting back and forth of the trephine demarcates a circular boundary and cuts through the anterior one-third of the cornea into the stroma.[41] The demarcated tissue is removed and the bare stroma is treated with 1 nmol US09 or non-targeting control (NTC) sdRNA.

Biomicroscopy slit lamp was performed on days 1, 2, 3, and 7 after wounding. US09 (Wnd-US09) promoted wound closure faster than NTC (Wnd-NTC). By day 2 there was an increase in wound closure with US09 treatment ($p < 0.01$) that was significant at each day tested ($p < 0.05$). By day 7 the US09-treated corneas were qualitatively clear compared to NTC treatment (Figures 1E and 1F).

To test the ability of the sdRNA to penetrate the wounded cornea, after nucleation of unwounded eyes from rabbits, the globes were wounded with a trephine as described above and corneas were excised and mounted on a collagen base. One nmol of non-targeting sdRNA

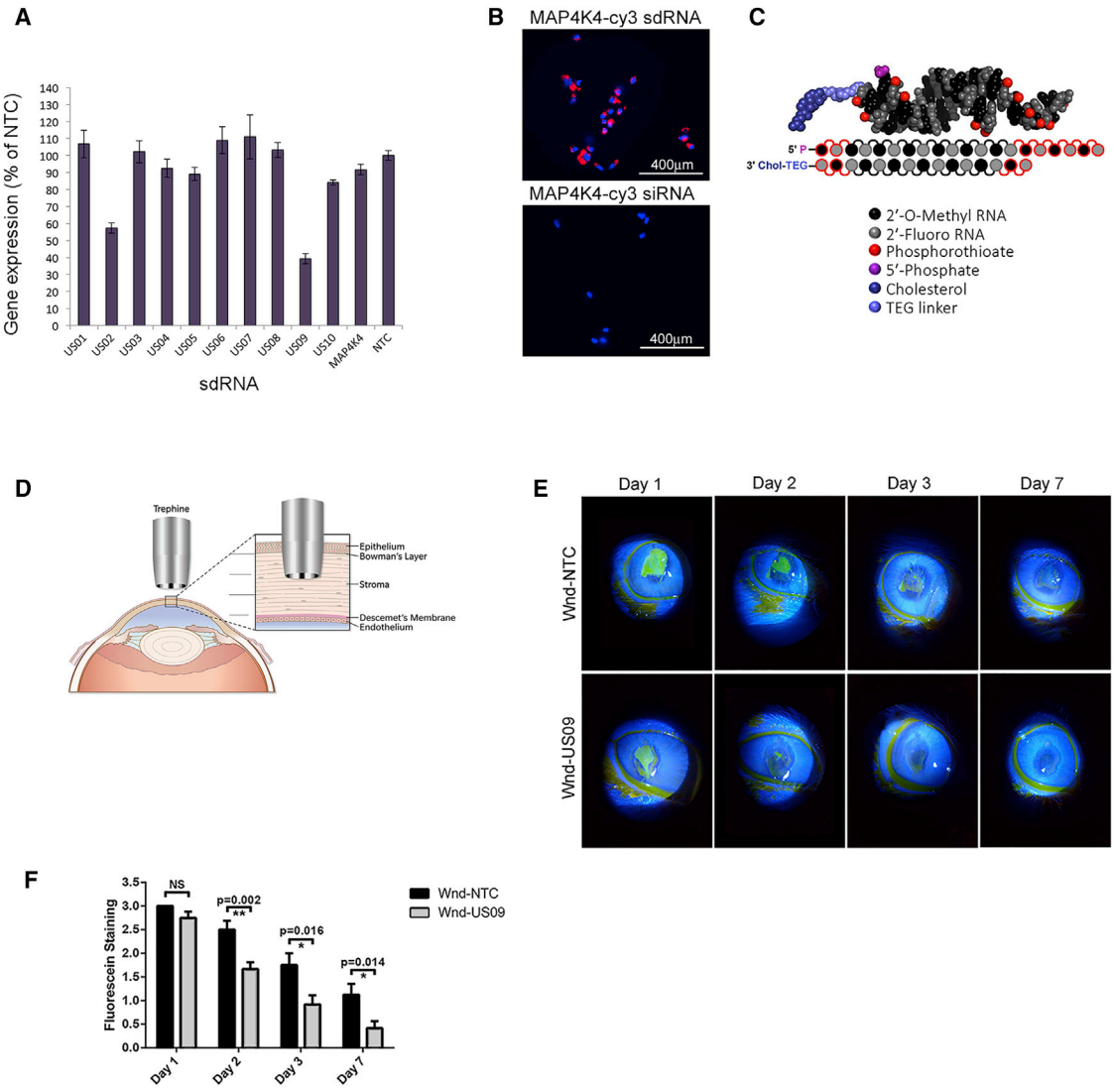

Figure 1. USP10 sdRNA Screening and *In Vivo* Corneal Wounding

(A) Primary rabbit corneal fibroblasts were treated with 1 μM of each sdRNA for 72 h, and USP10 expression was analyzed by qPCR. Rabbit GAPDH served as a reference gene. Knockdown efficiency was expressed as the percentage of non-targeting control (NTC). (B) Delivery of non-targeting Cy3-labeled sdRNA (MAP4K4-Cy3, 0.25 μM) into primary rabbit corneal fibroblasts, demonstrating efficient cellular uptake. Control cells were treated with the same dose of non-targeting Cy3-labeled siRNA (without cholesterol modification). Scale bars, 400 μm. (C) sdRNAs are asymmetric siRNAs, consisting of a 20-nt antisense strand and a 15-nt sense strand, in which all nucleotides are either 2′-fluoro (2′-F) or 2′-OMe modified. The 3′ terminal backbone is phosphorothioated (six linkages in antisense and two in sense). The 3′ end of the sense strand is conjugated to cholesterol. (D) Corneal wounding strategy. The human cornea is composed of five main layers, i.e., epithelium, Bowman's membrane, stroma, Descemet's membrane, and endothelium. Using a cylindrical blade called a trephine, a wound is made through one-third of the anterior portion of the cornea. The tissue within the trephine cut is excised with a blade and forceps. The bare stroma is treated with sdRNA. (E) Wound closure assessed by slit lamp. Wounded eyes treated with NTC (Wnd-NTC) or US09 (Wnd-US09) were treated with fluorescein drops and imaged by slit lamp on days 1, 2, 3, and 7 post-wounding. Images were analyzed for wound closure and rated from 0 to 3 (healed, no fluorescein to least healed, greatest fluorescein). (F) Wound closure was faster in Wnd-US09 compared to Wnd-NTC on days 2 ($p < 0.01$), 3 ($p < 0.05$), and 7 ($p < 0.05$). N = 6 rabbits per condition.

(MAP4K4 sdRNA-Cy3) was pipetted into the wounded stroma. Images were taken immediately at "time zero" on a dissecting scope, maintaining the sterility of the corneas. Corneas were imaged by live cell confocal microscopy at 2, 24, 48, and 72 h and at 168 h (7 days). The Cy3-sdRNA penetrated the bare stroma to 324 μm by 24 h. Total depth of the rabbit cornea is approximately 407 μm.[51] By 48 h the depth of the dye retreated to an average of 242 μm and remained at that depth until the final assay point of 7 days (Figure S2). Future studies will analyze sdRNA delivery to other parts of the eye *in vivo* over time and any potential systemic effects.

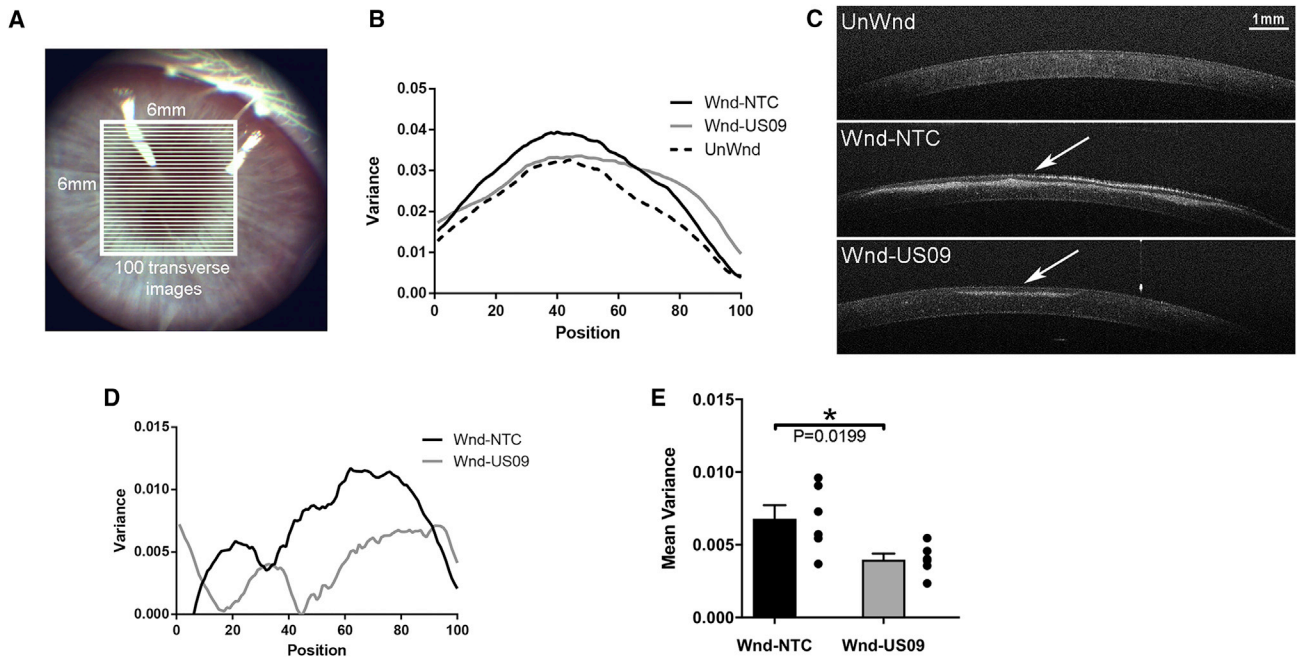

Figure 2. Quantitative Analysis after Wounding by OCT

At 6 weeks after wounding, rabbits were imaged by OCT after sedation and prior to sacrifice. 6 × 6-mm images were captured. (A) Representation of how images were partitioned into 100 optical slices in MATLAB. (B) The variance in each of 100 sections was quantified and averaged for all six animals (black, Wnd-NTC; gray, Wnd-US09; dotted line, UnWnd). (C) OCT images for each condition. Arrow denotes scar. Scale bar, 1 mm. (D) Variance: unwounded was subtracted from both Wnd-NTC and Wnd-US09). (E) All points in both conditions were averaged to create the mean variance (total of 10,000 points per rabbit, six rabbits per condition). US09 promotes a 41.5% reduction in scarring ($p < 0.05$).

Quantitative Analysis of Corneal Scarring by Optical Coherence Tomography

After 6 weeks, to quantify scarring, optical coherence tomography (OCT) images were analyzed for the variance of pixel intensities in the 6-mm wounded section of the cornea. Aberrations in the cornea (i.e., scarring) increase non-uniformity of pixel intensities in localized areas. To quantify this non-uniformity, we segmented the cornea in each image file into 100 equal parts (Figure 2A). For each segment the statistical variance (i.e., SD^2) of pixel intensities was calculated (Figure 2B). OCT images of the unwounded group (UnWnd), Wnd-NTC, and Wnd-US09 eyes are shown in Figure 2C. Next, UnWnd variance was subtracted from Wnd-NTC and Wnd-US09 to yield a clearer model of variance between the two treatments (Figure 2D). Finally, all points were reduced to the mean variance, which demonstrated a 41.5% decrease in scarring in Wnd-US09 corneas compared to Wnd-NTC (Figure 2E).

Immunohistochemistry for Fibrotic Markers

After OCT analysis, rabbits were sacrificed and eyes were enucleated. The cornea was excised from the globe and cut in half through the wound. To assess the protein expression of classic fibrotic markers, frozen sections were immunostained for collagen III, FN-EDA (also termed cellular FN), and α-SMA, all key markers of scarring.[52,53] For collagen III, compared to UnWnd, Wnd-NTC demonstrated a 276.2-fold increase in collagen III immunostaining ($p < 0.01$), which was reduced by 71.7% ($p < 0.05$) with Wnd-US09. The comparison between UnWnd and Wnd-US09 was not significant (Figures 3A and 3D). The increase in USP10 gene expression after wounding as assayed by qPCR was blunted by US09 (58.8%, $p < 0.01$ at days 1 and 2, and 91.2%, $p < 0.05$, at 6 weeks). The expression of USP10 does not decrease below unwounded levels even with US09 treatment after wounding. However, US09 significantly prevents upregulation of USP10 gene expression after wounding.

Similar to collagen III, Compared to unWnd, Wnd-NTC demonstrated a 8.33-fold increase in FN-EDA immunostaining ($p < 0.001$). Compared to Wnd-NTC, FN-EDA immunostaining was reduced by 53.8% ($p < 0.05$) in Wnd-US09. The comparison between UnWnd and Wnd-US09 was not significant (Figures 4A–4D). Finally, compared to UnWnd, Wnd-NTC demonstrated a 5.77-fold increase in α-SMA immunostaining ($p < 0.05$), which was reduced by 83.6% ($p < 0.05$) in Wnd-US09. The comparison between UnWnd and Wnd-US09 was also not significant (Figures 5A–5D). Next, we counted cell proliferation into the wound and corneal thickness (see Materials and Methods). These data demonstrate that cell proliferation into the wound in Wnd-US09 corneas is similar to UnWnd tissue, whereas Wnd-NTC is significantly increased Figure 5E ($p < 0.01$). Cell proliferation below the wound in the stroma down to the endothelial layer was invariant between conditions (Figure 5F). Corneal thickness over the entire cornea in Wnd-US09 treated

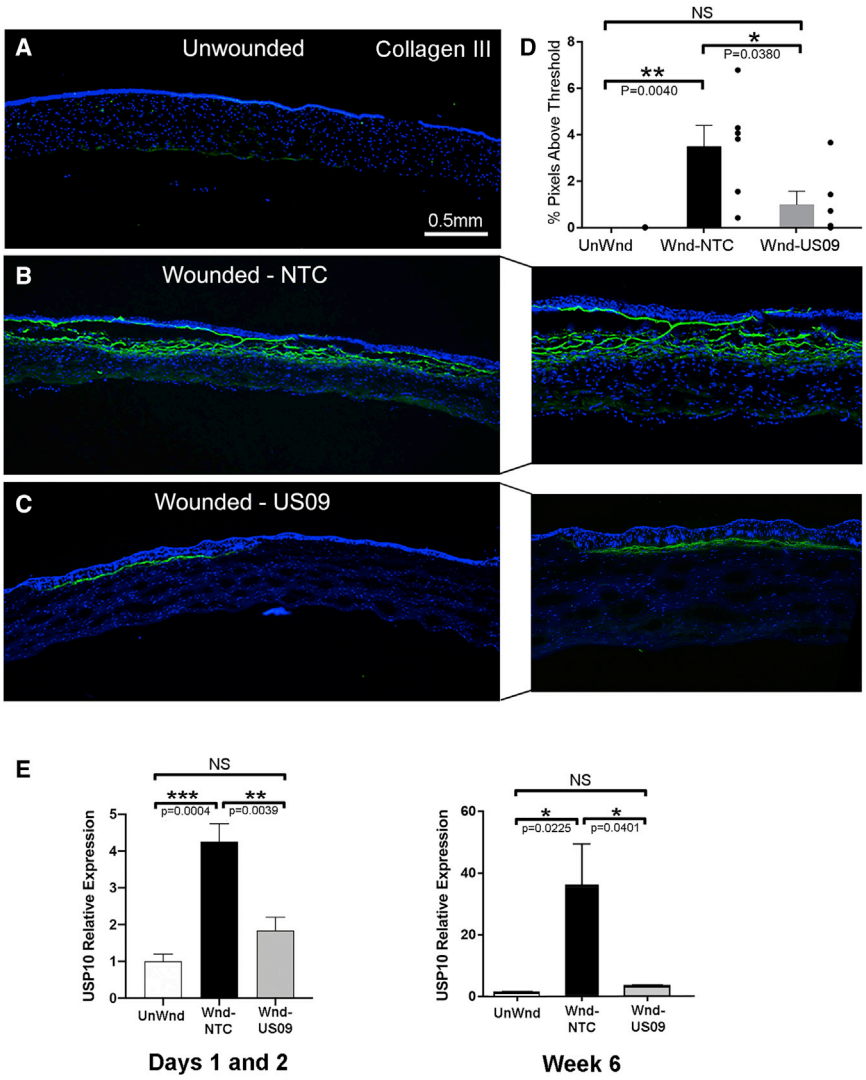

Figure 3. Immunohistochemical Analysis of Collagen III after Wounding

(A–C) Frozen sections of corneas 6 weeks after wounding were immunostained for collagen III (green), DAPI (blue). (A) UnWnd, (B) Wnd-NTC with magnified inset, and (C) Wnd-US09 with magnified inset. Scale bar, 0.5 mm. (D) Compared to UnWnd, Wnd-NTC demonstrated a 276.2-fold increase in collagen III immunostaining ($p < 0.01$), which was reduced by 71.7% ($p < 0.05$) with US09 treatment. The comparison between UnWnd and Wnd-US09 was not significant. (E) By qPCR, days 1 and 2 combined, compared to UnWnd, Wnd-NTC demonstrated a 4.26-fold increase in USP10 gene expression ($p < 0.001$). Compared to Wnd-NTC, USP10 expression with Wnd-US09 treatment was reduced by 56.8% ($p < 0.01$). N = 4 rabbits per condition. At 6 weeks, compared to UnWnd, Wnd-NTC demonstrated a 35.7-fold increase in USP10 gene expression ($p < 0.05$). Compared to Wnd-NTC, USP10 expression with Wnd-US09 treatment was reduced by 91.2% ($p < 0.05$). N = 6 rabbits per condition.

corneas was not significantly different from UnWnd parameters (Figure 5G). Wnd-NTC compared to UnWnd was also not significant but trended toward being thinner ($p = 0.05$). Taken together, these data demonstrate that a one-time treatment of sdRNA targeting USP10 after wounding significantly reduces scarring at 6 weeks.

Immune Marker CD45

To begin to study the infiltration of immune cells into the wound, we repeated the wounding experiment to analyze $CD45^+$ staining and collected tissue at days 1, 2, and 3 to compare to 6 weeks. As shown in Figures 6A–6I), by 1 day after wounding, $CD45^+$ immune cells populate the wound in both Wnd-NTC and Wnd-US09 conditions. However, overall, by day 3 there is a clear difference between Wnd-NTC and Wnd-US09; that is, in the Wnd-NTC tissue, there are more $CD45^+$ cells and, importantly, they are distributed throughout the stroma in and below the wound, whereas in the Wnd-US09 tissue, they are localized to the anterior stroma only (arrows). (At this early time point, the epithelium often falls off during immunostaining of wounded tissue, as the tissue is not fixed and the wound margin is still fragile.) At 6 weeks, the same distribution is observed (Figures 6J–6L, with magnified panels). Figure 6M shows the quantification of $CD45^+$ cells in the three conditions during the first 3 days, at 6 weeks, and with the data grouped. At days 1–3, compared to UnWnd, Wnd-NTC demonstrated a 7.1-fold increase in $CD45^+$ immunostaining. Comparing Wnd-NTC to Wnd-US09, $CD45^+$ staining was reduced by 46.2% ($p < 0.05$). At 6 weeks, compared to UnWnd, Wnd-NTC demonstrated a 3.4-fold increase in $CD45^+$ immunostaining. Comparing Wnd-NTC to Wnd-US09, $CD45^+$ staining was reduced by 55.2% (trending toward significant, $p = 0.06$). For the grouped data, compared to UnWnd, Wnd-NTC demonstrated a 4.66-fold increase in $CD45^+$ immunostaining ($p = 0.001$), and comparing Wnd-NTC to Wnd-NTC $CD45^+$ staining was reduced by 51.0% ($p < 0.01$). The comparison between UnWnd and Wnd-US09 was not significant. In summary, US09 reduces $CD45^+$ cell infiltration after wounding.

Apoptosis after Wounding

After wounding in the cornea, local cells in the stroma in and beneath the wound apoptose.[54,55] In response to wounding and apoptosis, neutrophils and macrophages ($CD45^+$ cells) infiltrate the wound as shown in Figure 6. We found that US09 treatment significantly prevented apoptosis after wounding, when comparing Wnd-NTC to Wnd-US09 (65.0% reduction on day 1, $p < 0.01$; 65.0% reduction on day 2, $p < 0.05$) (Figure 7). This may be a key to the anti-scarring activity of US09. Less apoptosis will attract less leukocyte infiltration with diminished scarring.

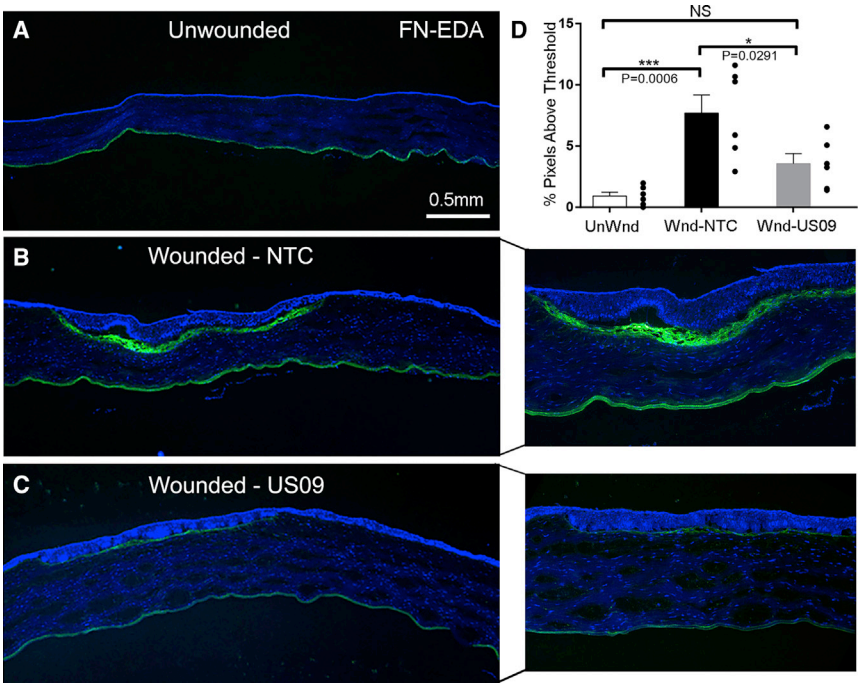

Figure 4. Immunohistochemical Analysis of FN-EDA after Wounding

(A–C) Frozen sections of corneas 6 weeks after wounding were immunostained for fibronectin-EDA (FN-EDA, green), DAPI (blue). (A) UnWnd, (B) Wnd-NTC with magnified inset, and (C) Wnd-US09 with magnified inset. Scale bar, 0.5 mm. (D) Compared to UnWnd, Wnd-NTC demonstrated a 8.33-fold increase in FN-EDA immunostaining ($p < 0.001$). Compared to Wnd-NTC, FN-EDA immunostaining after Wnd-US09 treatment was reduced by 53.8% ($p < 0.05$). The comparison between UnWnd and Wnd-US09 was not significant. N = 6 rabbits per condition.

DISCUSSION

In this study, we demonstrate that one application of self-deliverable siRNA targeting the DUB USP10 (US09) is a novel method to significantly reduce scarring in the cornea. This was shown by faster wound closure (Figure 1), a decrease in the variance of pixels in OCT images (Figure 2), a reduction in fibrotic markers to a level that was not significantly different from unwounded tissue (Figures 3, 4, and 5), a reduction in $CD45^+$ cells (Figure 6), and a reduction in the apoptotic response to wounding (Figure 7). Based on our data and the known functions of USP10, we hypothesize that USP10 plays a central role in wound healing by regulating apoptosis in a context-dependent manner, i.e., pro-apoptosis directly after wounding, and anti-apoptosis (pathological myofibroblast development) later in wound healing.

We identified the role of USP10 in myofibroblasts through the utilization of a unique cellular wounding model. The extracellular protease system, urokinase-type plasminogen activator (uPA)/uPA receptor (uPAR), generates plasminogen and plasmin on the cell surface. The receptor, uPAR, is glycosylphosphatidylinositol (GPI) linked, and it coordinates with the cytoskeleton intracellularly through binding to integrins. Whereas addition of uPA to the cell induces cell motility, and high levels of uPA/uPAR/integrin binding promotes cancer cell invasion,[56] we found that uPA or uPAR knockdown in primary human corneal fibroblasts induced an adhesive, myofibroblast phenotype with dramatically increased cell surface expression of $\alpha_v\beta_5$ and highly organized α-SMA.[29] Further investigation proved that it was not gene expression changes that increased integrin $\alpha_v\beta_5$, but instead a post-translational decrease in ubiquitination of integrin β_5.[28] Thus, we leveraged this finding and performed RNA-seq on uPA siRNA-treated cells to find novel targets for the generation of a pathological myofibroblast phenotype without the addition of TGF-β. In support of this strategy, uPAR knockout mice develop dermal scarring and lung and myocardial fibrosis.[57–59] From the RNA-seq data we found that the DUB USP10 was important for myofibroblast development as it deubiquitinates β_1 and β_5 integrins, specifically, $\alpha_v\beta_5$ and β_1 but not $\alpha_v\beta_3$, leading to an accumulation of cell surface integrin and subsequent activation of local TGF-β.[28,29] Furthermore, after wounding in an *ex vivo* corneal wounding model, USP10 is significantly upregulated in the stroma, and USP10 siRNA reduces or eliminates fibrotic markers.[28]

As stated in the Introduction, USP10 is also a DUB for p53 and thus plays a role in regulating apoptosis. Our new working model (Figure 8) that integrates both our published work on integrins and our current *in vivo* data on apoptosis and immune cell infiltration is that directly after wounding, as stimulated by USP10 upregulation,[28] USP10/p53 activity in the nucleus is dominant, leading to less p53 ubiquitination and stabilizing pro-apoptotic p53.[42] Local cell apoptosis induces mast cell activation and the infiltration of neutrophils and macrophages into the wound.[60–62] Activated keratocytes peripheral to the apoptotic zone proliferate to repopulate the wound margin. These cells and infiltrating bone marrow-derived fibrocytes[63] differentiate into myofibroblasts in the next few days. In this second phase we propose that USP10 favors binding to cytosolic proteins such as G3BP1/2 and integrins directing USP10 away from nuclear p53. USP10 binding to G3PB2 in the cytosol induces p53 cytoplasmic localization, ubiquitination, and degradation.[64] The connection between G3BP1/2 and USP10-mediated integrin deubiquitination is unknown; however, G3BP1/2 downregulation inhibits Scr/FAK/ERK signaling, suggesting a USP10/integrin/G3BP complex and coordination between these proteins.[65] Germane to this model is a recent study in which USP10/TRAF4 binding induced p53 ubiquitination and cytosolic degradation (similar to the USP10/G3BP interaction), leading to a fibroproliferative response and keloid formation.[66] Thus, we suggest that the switching of USP10 functions from pro-apoptotic to anti-apoptotic is context-dependent and depends on 3D environmental cues in the wound bed.

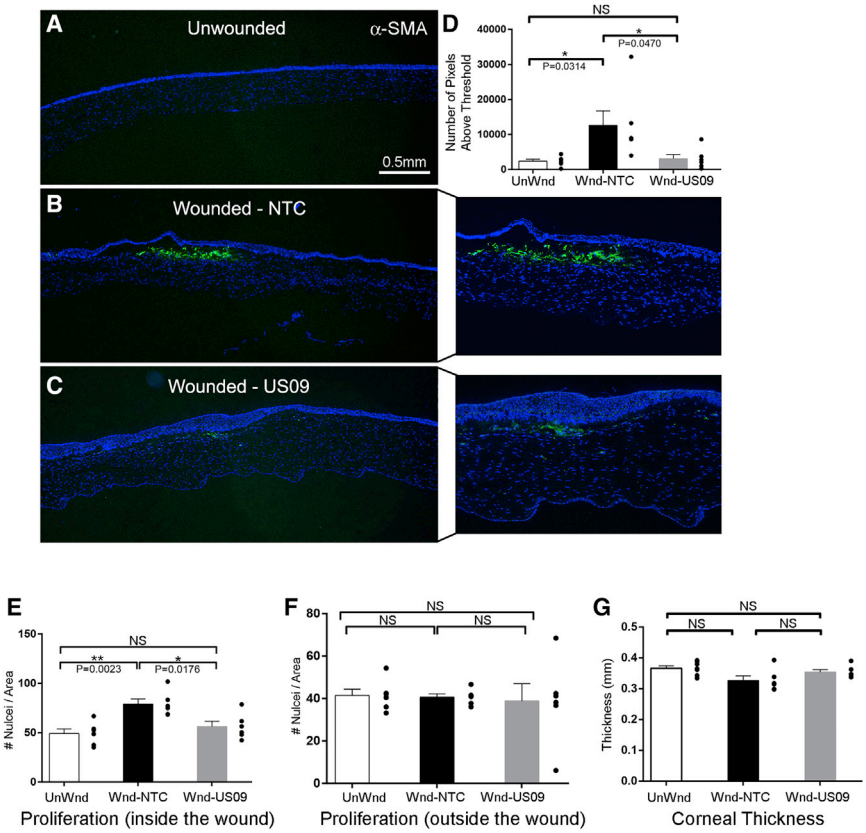

Figure 5. Immunohistochemical Analysis of α-SMA, Cell Proliferation, and Thickness after Wounding

(A–C) Frozen sections of corneas 6 weeks after wounding were immunostained for α-SMA (green), DAPI (blue). (A) UnWnd, (B) Wnd-NTC with magnified inset, and (C) Wnd-US09 with magnified inset. Scale bar, 0.5 mm. (D) Compared to UnWnd, Wnd-NTC demonstrated a 5.77-fold increase in α-SMA immunostaining ($p < 0.05$). Compared to Wnd-NTC, α-SMA immunostaining after Wnd-US09 treatment was reduced by 83.6% ($p < 0.05$). The comparison between UnWnd and Wnd-US09 was not significant. (E and F) Cell proliferation was analyzed by the object counter plugin in ImageJ software. "Inside the wound" is denoted by the anterior cornea demarcated by the collagen III scar. "Outside the wound" is the posterior cornea beneath the scar. These counts were normalized by the total area of each portion to generate a nuclei density measurement. (E) Compared to UnWnd, Wnd-NTC demonstrated a 1.61-fold increase in cell proliferation ($p < 0.01$). Compared to Wnd-NTC, cell proliferation after Wnd-US09 treatment was reduced by 29.9% ($p < 0.05$). The comparison between UnWnd and Wnd-US09 was not significant. (F) Cell proliferation below the scar, in the stroma down to the endothelium. All relationships were not significant. (G) Corneal thickness was measured at pixel resolution in these thresholded images as the distance across the nonzero region, and thickness is averaged across the entire cornea. Wnd-NTC trended toward a slight decrease in thickness ($p = 0.05$). Wnd-US09 treatment restored corneal thickness to non-wounded parameters. N = 6 rabbits per condition.

We found that directly after wounding, local apoptosis is mediated by USP10, as US09 significantly diminished TUNEL (terminal deoxynucleotidyltransferase [TdT]-mediated deoxyuridine triphosphate nick end labeling)$^+$ cells. We hypothesize that reduced apoptosis led to less CD45$^+$ cell infiltration. Studies in the cornea show that blocking neutrophil invasion is the mechanism by which stem cell treatment in the cornea reduces scarring.[67] Also, less inflammatory cells reduce myofibroblast differentiation because inflammatory cells secrete growth factors, such as TGF-β.[68,69] In addition, US09 may remain long enough in the ECM to prevent USP10/integrin activity in proliferating fibroblasts, reducing α-SMA organization and pathological cell adhesion. Together, these USP10-mediated functions (apoptosis and integrin stabilization) appear to be a central organizer of scarring.

In general, there is little known about the regulation of myofibroblasts and cell surface integrin expression through DUB activity and the resulting link to disease. For the connection between DUBs and myofibroblasts, stellate cell activation induces the DUB UCHL1, and knockdown of UCHL1 blocks progression of CCl_4-induced fibrosis in mice.[70] Furthermore, pan-inhibition of DUBs with the DUB inhibitor PR-619 ameliorates renal fibrosis through the SMAD-4 pathway.[71] In terms of DUBs and integrins, the DUB ataxin-3 regulation of integrin α_5 is a critical component of the neurological disorder Machado-Joseph disease.[72,73] More widely, DUB biology, as well as a focus on DUBs as drug targets, represents an expanding field of study. DUBs are being targeted for both cancer and neurodegenerative diseases.[74,75] For USP10 specifically, a recent discovery using a protein engineering strategy for the rational design of DUB inhibitors found a sequence that when expressed as a cDNA directly targets USP10's DUB activity.[76] Future studies in our laboratory will dissect the different functions of USP10's structural domain and DUB activity and their relative contributions to scarring.

Because of the accessibility of the eye, RNAi therapy has made significant progress in clinical outcomes for eye diseases and, in general, gene knockdown with eye drops or by injection rivals the success of antibody therapies that have the challenge of being quickly diluted by tears, especially for anterior surface indications. Several new RNAi therapies target disease pathways for ocular indications such as caspase-2 for anterior ischemic optic neuropathy, hypoxia for neovascular age-related macular degeneration and diabetic retinopathy, β_2-adrenergic activity for glaucoma, and TRPV1 for dry eye, to name of few.[77] As may be expected, dosing the eye does not induce significant systemic effects.[44,78–81] Many RNAi-based therapies are in various stages of clinical trials for multiple indications, with the use of modified siRNA conjugates becoming a dominant therapeutic modality.[82] Other RNAi-based therapies for hepatitis C and various cancers are also in clinical trials.[77] Specific to scarring therapies for

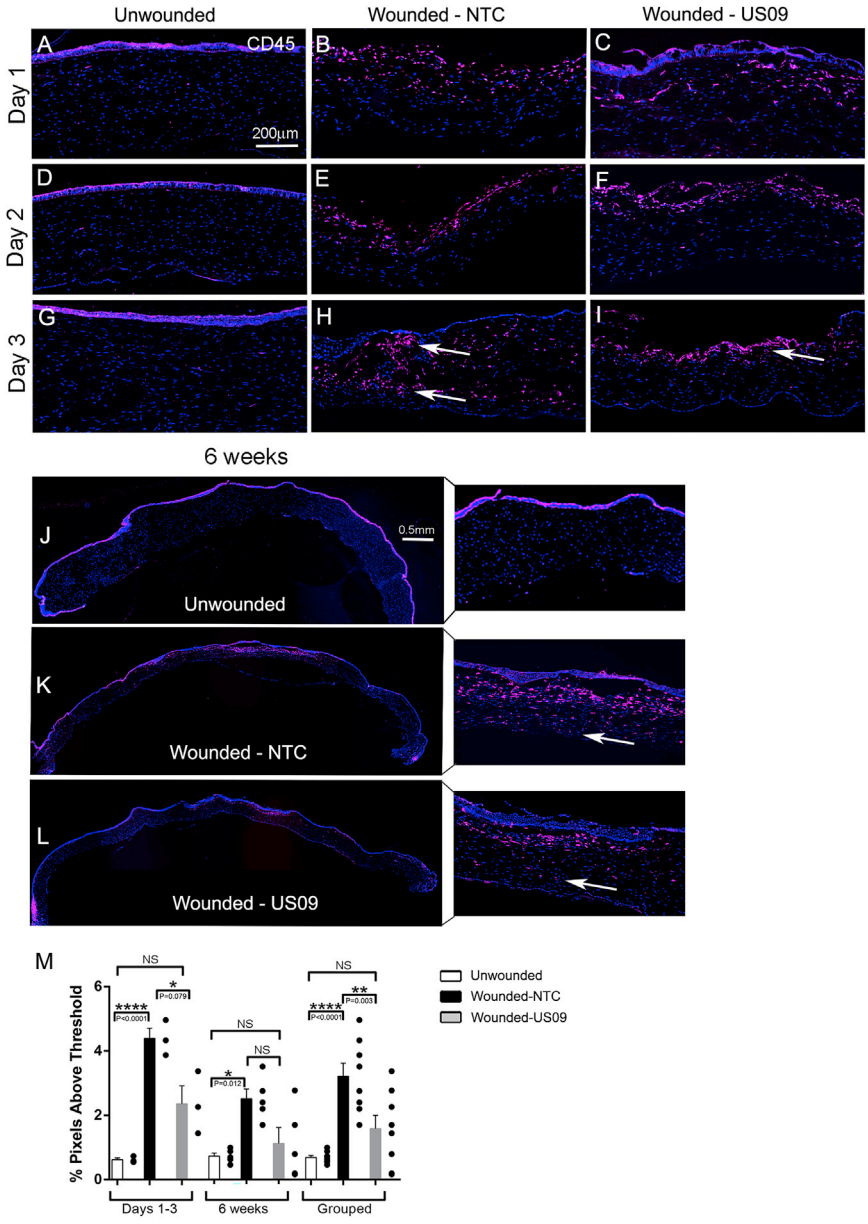

Figure 6. CD45⁺ Cell Infiltration after Wounding

(A–L) Frozen sections of corneas at days 1, 2, and 3 and 6 weeks after wounding were immunostained for CD45⁺ (red), DAPI (blue). (A–C) day 1, (D–F) day 2, (G–I) day 3 (scale bar, 200 μm), and (J–L) 6 weeks with magnified inset (scale bar, 0.5 mm). (A, D, G, and J) unwounded; (B, E, H, and K) wounded-NTC; and (C, F, I, and L) wounded-US09. (M) At days 1–3, compared to UnWnd, Wnd-NTC demonstrated a 7.1-fold increase in CD45⁺ immunostaining. For Wnd-NTC compared to Wnd-NTC, CD45⁺ staining was reduced by 46.2% ($p < 0.05$). At 6 weeks, compared to UnWnd, Wnd-NTC demonstrated a 3.4-fold increase in CD45⁺ immunostaining. Comparing Wnd-NTC to Wnd-US09, CD45⁺ staining was reduced by 55.2% ($p = 0.06$). For the grouped data, compared to UnWnd, Wnd-NTC demonstrated a 4.66-fold increase in CD45⁺ immunostaining ($p = 0.001$); comparing Wnd-NTC to Wnd-NTC, CD45⁺ staining was reduced by 51.0% ($p < 0.01$). The comparison between UnWnd and Wnd-US09 was not significant. US09 reduces CD45⁺ cell infiltration. N = 3 rabbits per condition for days 1–3. N = 5 rabbits per condition for the 6-week time point. N = 8 rabbits per condition for grouped data.

the eye is a study in rabbits for the knockdown of the *MTRF* (myocardin-related transcription factor) gene that is a master regulator of actin genes. RNAi to *MRTF* reduced scarring in the fibrotic "bleb" made during the glaucoma filtration surgery to relieve pressure in the eye.[83,84] Several other gene knockdown strategies for ocular scarring are also being tested in animals.[1,9–11,14]

In this study, we used the fully modified siRNA conjugate to achieve maximal activity and longevity of the effect *in vivo*.[48] Regarding the possibility of off-target effects, the asymmetric (20/15) chemically modified siRNA used in this study was designed to avoid any sequence identity with other rabbit genes within the 2–18 region of the anti-sense strand. The closest rabbit sequence identified in the rabbit transcriptome has four mismatches in the siRNA seed region, which completely excludes the possibility of a sequence-specific off-target effect caused by an anti-sense strand of siRNA (Figure S3). Furthermore, since the sdRNA is delivered to cells in the asymmetric duplex form, the anti-sense strand itself cannot have any off-target effects, as it does not efficiently enter the RNA-induced silencing complex (RISC). The possible off-target effects caused by a sense strand are excluded by (1) its length (15, too short for RISC) and (2) having 2′-*O*-methylation (2′-OMe) modifications in positions 2 and 14, which inhibit RNAi activity.

US09 does not achieve complete gene knockdown *in vitro* (Figures 1A and S1). Incomplete knockdown can be explained by a variety of reasons, including the presence of mRNA isoforms detectable by the qPCR probes that are not affected by the sdRNA, or by the nuclear localization of mRNA.[85] However, it is not always advantageous to have complete knockdown. We have consistently observed that small changes in USP10 expression relate to large phenotypic changes in cells.[28] In addition, our goal in this study was achieved by preventing the upregulation of USP10 after wounding, instead of knocking down USP10 below control levels observed in unwounded tissue (Figure 3E). Dosing US09 twice, directly after wounding and at 6, 12, or 24 h after wounding, may totally prevent apoptosis and myofibroblast differentiation by targeting a wave of infiltrating cells that are not initially present. Another option is a slower delivery mechanism by absorbing US09 to a substrate and

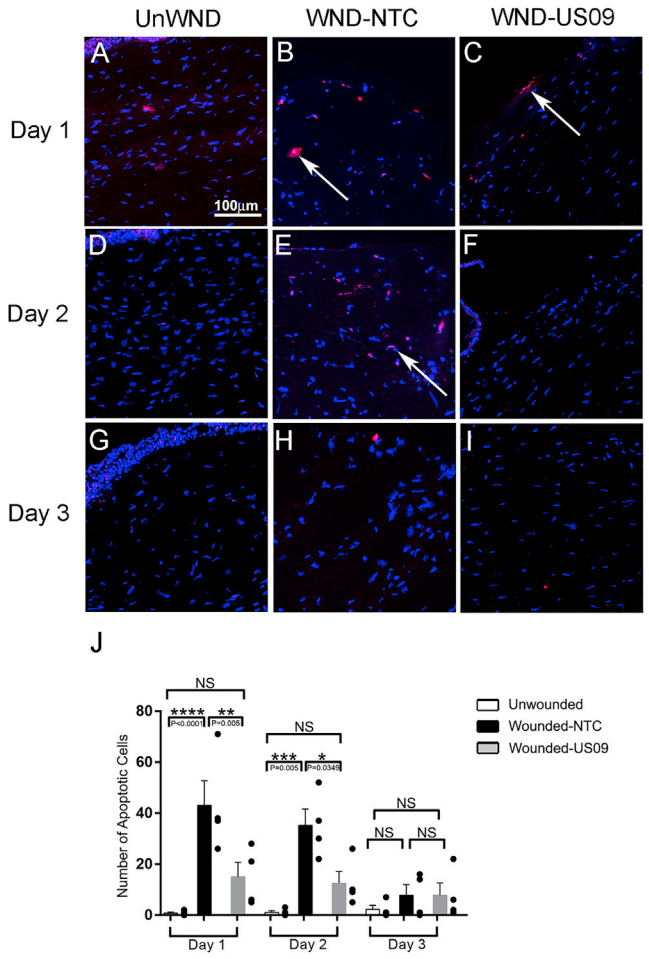

Figure 7. Apoptosis after Wounding

(A–I) Apoptotic cells were detected with TUNEL assay on days 1 (A–C), 2 (D–F), and 3 (G–I) in unwounded conditions and after wounding. (A, D, and G) UnWnd; (B, E, and F) Wnd-NTC; and (C, F, and I) Wnd-US09. (J) On day 1, US09 treatment reduced apoptosis 65.0% from 43.0 ± 9.7 to 15.0 ± 5.7 cells per section in the wound ($p < 0.01$). On day 2, US09 treatment also reduced apoptosis 65.0% from 35.3 ± 6.4 to 12.5 ± 4.6 cells per section in the wound ($p < 0.05$). Apoptosis was not significant between conditions by day 3. Scale bar, 100 μm. N = 4 rabbits per condition per time point.

covering the eye for a 24-h period. Finally, the activity of US09 can be further enhanced by backbone modification optimization. Future studies with longer time points (3 and 6 months) will determine how the scars resolve in each condition. In summary, we have demonstrated a novel anti-scarring method through the knockdown of USP10. We predict that this strategy can be more broadly applied to prevent scarring in other, non-ocular tissues.

MATERIALS AND METHODS

Sequencing of Rabbit Corneal USP10

Rabbit corneas were obtained from Pel-Freez Biologicals (Rogers, AR, USA). Rabbit primary corneal keratocytes were derived from the corneal stroma as previously described.[86] Total RNA was isolated with TRIzol reagent (Invitrogen) or using a PureLink RNA mini kit (Invitrogen). RNA was sent to ACGT (Wheeling, IL, USA). The RNA samples were evaluated by Qubit fluorometry and an Agilent 2100 Bioanalyzer. First-strand cDNA was constructed using the Mint-2 cDNA synthesis kit. The cDNA samples were evaluated by fluorometry and agarose gel electrophoresis. PCR was performed on first-strand cDNA, using PrimeSTAR GXL DNA polymerase and primers designed specifically for this study. All PCR products were evaluated by fluorometry and agarose gel electrophoresis. The "rabbit" PCR products were purified using Agencourt AMPure XP beads and evaluated by fluorometry. Purified PCR products were fragmented by ultrasonication to an average 250-bp target fragment size. Uniquely barcoded sequencing libraries were constructed from fragmented DNA, using the NEXTflex Rapid DNA sequencing kit as per the manufacturer's instructions. Appropriate quality control analysis was performed at every step. Final libraries were assessed by Qubit fluorometry and an Agilent 2100 Bioanalyzer. Final libraries were combined with compatible libraries from other projects, and loaded onto a HiSeq 300 cycle flow cell to generate 150PE reads. Enough sequence was generated to provide at least 0.5 million reads per sample, with Q30 quality (average per read) sequence data. The raw Illumina reads were de-multiplexed and converted into fastq format. Low-quality ($Q < 30$) and short reads ($N < 50$) were filtered out. The trimmed and filtered reads were *de novo* assembled to generate contigs. The contigs were analyzed and identified using BLAST, and a final assembly was constructed (GenBank: MN927131). The trimmed and filtered reads were aligned to the reference sequence of the predicted USP10 gene based on the results of the BLAST analysis, and a variant report was generated.

The resulting *de novo* sequence for rabbit corneal USP10 was aligned with predicted RefSeq variants XM_002723256.1 and XM_002723256.2. The common region with 99% identity covering partial 3′ UTR and most of the coding sequence, with the exception of three initial exons, was extracted as a consensus sequence for sdRNA design. The regions containing a few nucleotide mismatches with the database variants were avoided.

sdRNAs

sdRNAs are the fully chemically modified asymmetric siRNA-cholesterol conjugates.

For the identification of the active sdRNAs against rabbit USP10 gene 10 lead candidates were predicted by the published algorithm.[49] The designed sequences are listed in Figure S4. For the primary screening, sdRNAs were synthesized as separate guide and passenger strands (TriLink Biotechnologies, San Diego, CA, USA) and dissolved in sterile RNase-free, DNase-free water for injection (CalBiochem, 4.86505) at 200 μM. Duplexes were annealed by mixing equal volumes of the strand solutions, followed by heating to 95°C for 5 min and allowing to cool gradually to room temperature. The quality of duplex formation was tested by using native gel electrophoresis (Figure S5). The sdRNA solutions were stored at −80°C. Prior to use, the sdRNA stock

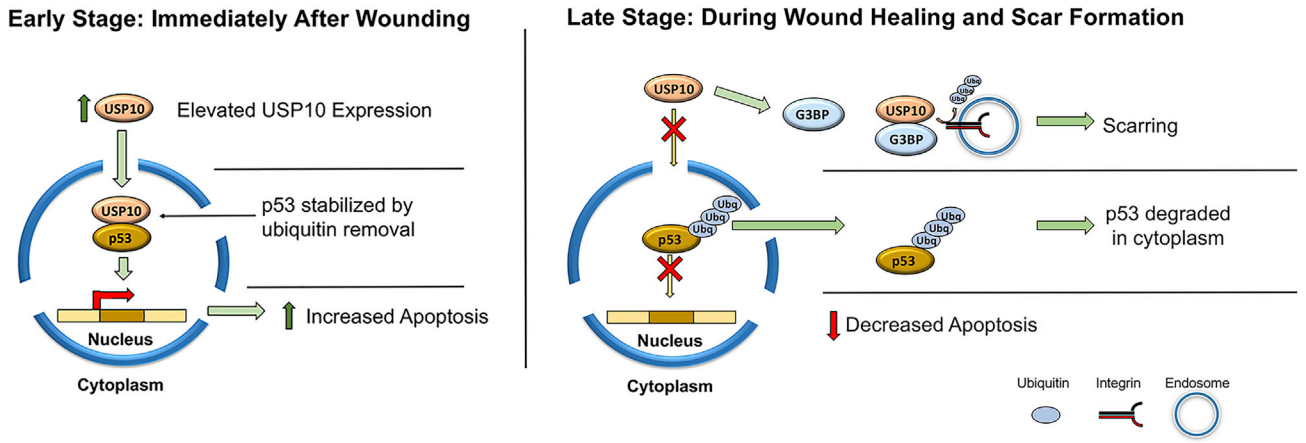

Figure 8. Working Model for Divergent Roles of USP10 as Wound Healing/Scarring Progresses

Left panel: immediately following a corneal stromal injury, resident keratocytes adjacent to the wound undergo apoptosis. USP10, which is upregulated in the wound,[28] plays a role in apoptosis by deubiquitinating p53. p53 stabilization promotes tumor suppressor/pro-apoptotic gene expression and signaling, resulting in controlled cell death. Knockdown of USP10 by US09 treatment diminished the apoptotic response. Right panel: USP10 deubiquitylates α_v integrins, leading to cell surface accumulation, myofibroblast persistence, and activation of TGF-β.[28] Our working hypothesis is that sustained upregulation of stress-response genes, such as the G3BP proteins (known binding partners of USP10),[92] competes for interaction with available USP10 in the cytoplasm, switching USP10's function from pro-apoptotic to anti-apoptotic. This model is supported by data in prostate cancer cells and in keloid scars, in which USP10 switches from a pro-apoptotic role in the nucleus to binding to stress-related proteins in the cytoplasm.[64,66] Other studies have demonstrated a role for G3BP1/2 in regulating integrin signaling molecules (Src, FAK, and ERK).[65] Taken together, we predict that in the early stages of wounding, USP10 promotes apoptosis and subsequent immune cell infiltration, while in the later stages of wound healing (scar formation), USP10 is directed by its binding partners to promote myofibroblast survival (inhibition of apoptosis) and differentiation (α_v integrin upregulation, enhanced cellular adhesion/contractility). We have demonstrated that knockdown of USP10 gene expression after wounding significantly reduces scarring.

solution was heated to 37°C for 5 min, vortexed, and briefly spun down. The selected in primary *in vitro* screening sdRNA sequence (US09) was synthesized at the 10 μmol scale (TriLink), and the same sequence with 5′-terminal vinyl-phosphonate and non-targeting control were synthesized at the 10 μmol scale by ChemGenes (Wilmington, MA, USA). These duplexes were formed at 200 μM final concentration in sterile PBS. The final sequences used for the experiments are listed in Table 1.

RNA Extraction and qPCR

Rabbit corneas were obtained from Pel-Freeze Biologicals (Rogers, AR, USA). Keratocytes were isolated from corneas and differentiated into fibroblasts as previously described.[86] Primary rabbit corneal fibroblasts were maintained in DMEM/F12 medium supplemented with 10% fetal bovine serum (FBS) and penicillin/streptomycin solution (Gibco). Cells were cultured for 1–2 weeks and passaged once 24 h prior to transfection. For the qRT-PCR assay in Figures 1A and S1 (sdRNA screening), cells were trypsinized and mixed with oligonucleotides in reduced serum medium DMEM with 3% FBS at a final concentration of 1 μM sdRNA. Cells were incubated for 72 h and then harvested. Total RNA from primary corneal fibroblasts was purified with a PureLink RNA 96 kit (Invitrogen) according to the manufacturer's recommendations and was added as a template into a one-step multiplex qRT-PCR assay using Quanta qScript XLT ToughMix with ROX dye (VWR). For that, 1 μL of total RNA was mixed with the reagent and primer-probe mixes for rabbit USP10 and reference gene GAPDH in a 10-μL reaction. The cycling parameters were as recommended by Quanta. The primer-probe mix for GAPDH labeled with VIC (4,7,2′-trichloro-7′-phenyl-6-carboxyfluorescein) was from TaqMan (Oc03823402_g1), and the primer-probe mix for rabbit USP10 labeled with FAM (6-carboxyfluorescein) was specifically designed for the generated rabbit corneal sequence and synthesized by Thermo Fisher Scientific. The sequences were as follows: primers, 5′-CTGCATTTTCGGTGGACACA-3′ and 5′-TGGCCGATTCTTTCGAACTCT-3′; MGB probe covering exon 11–12 junction of XM_002723256.2, 5′-TCAGGTCTGTGGTT TACC-3′.

For the qRT-PCR assays in Figure 3E, immediately after sacrifice, eyes were enucleated and corneas were excised from the globes. The cornea was cut in half through the wound and the wounded section was excised and put directly into TRIzol reagent (Invitrogen). A PureLink RNA mini kit (Invitrogen) was used to extract total RNA. Further purification of both tissue and primary cell RNA was performed with a Monarch PCR & DNA cleanup kit (New England Biolabs). cDNA was generated from 1 μg of total RNA in a 20-μL reaction using iScript reverse transcription supermix for qRT-PCR (Bio-Rad). The qRT-PCR was prepared in 10-μL reactions with iTaq Universal SYRB Green supermix (Bio-Rad) with 1 μL of cDNA and 500 nM each primer. The cycling parameters used were 95°C, 10 min; 40 cycles of 95°C, 15 s; 60°C, 60 s. Primers used were as follows: USP10 (IDT), 5′-AGAGCGCCTCCCTCCCTGCC-3′, 5′-GGTCCTCGGATGCCGGAACC-3′; GAPDH (IDT), 5′-GAGTG AACGGATTTGGCCGC-3′, 5′-TTGATGTTGGCGGGATCTCG-3′.

Table 1. Sequences Used in This Work

	Passenger Strand	Guide Strand
US09	fC.mA.fG.mA.fA.mG.fC.mU. fG.mA.fU.mC.fA#mA#fA-Chol	PmU.fU.mU.fG.mA.fU.mC.fA.mG.fC.mU. fU.mC.fU#mG#fA#mC#fA#mG#fC
NTC	fU.mU.fA.mC.fA.mU.fG.mU. fU.mU.fU.mC.fC#mU#fA-Chol	PmU.fA.mG.fG.mA.fA.mA.fA.mC.fA.mU. fG.mU.fA#mA#fA#mC#fC#mA#fA

The modifications are as follows: m, 2′-OMe; f, 2′-fluoro; #, thiophosphate; Chol, cholesteryl-TEG.

Ex Vivo Corneal Tissue Culture

This method of *ex vivo* organ culture has been previously described.[28,41] Briefly, after enucleation of the eyes, a 6-mm trephine was used to wound the center of the cornea. The wound penetrated the epithelium and anterior stroma without making a full-thickness wound through the entire cornea, as described below for the *in vivo* experiments. The demarcated tissue was removed. Corneas were mounted on an agar base and wet with PBS. One nmol (5.0 μL) of non-targeting Cy3-labeled sdRNA (MAP4K4-cy3, Advirna) was pipetted into the wound and imaged immediately under a dissection scope (Accu-Scope, Commack, NY, USA). Cell culture lids remained attached during imaging to maintain sterility. Four mL of supplemented serum-free medium[28] was added to the plate, maintaining corneas at an air-liquid interface at the limbal border in 5% CO_2 at 37°C. Corneas were wet every 24 h with conditioned media. Media were changed every 48 h (Cy3-sdRNA was not re-added). At 2 h, day 1, day 2, day 3, and day 7 corneas were imaged by live-cell confocal microscopy (Zeiss, LSM780) (Figure S2).

Animal Studies

We used 12 female New Zealand White rabbits[87] (Charles River), each 12–15 weeks old and weighing 2.5–3.0 kg. The Institutional Animal Care and Use Committee of SUNY Upstate Medical University approved the study. General anesthesia in rabbits was given by an intramuscular injection of ketamine hydrochloride (100 mg/mL) given at 40 mg/kg and xylazine hydrochloride (100 mg/mL) given at 6 mg/kg along with an injection of buprenorphine SQ (slow release) (1 mg/mL) given at 0.1 mg/kg for pain control. Local anesthesia was also given with two drops of topical 0.5% proparacaine hydrochloride (Alcon Laboratories, Fort Worth, TX, USA). At euthanasia, anesthesia was administered as above prior to 1 mL of Fatal Plus IV (pentobarbital sodium, 390 mg/mL). In each rabbit, the right eye was wounded. The central area of the anterior cornea was demarcated with a 6-mm trephine. The circular area that was demarcated was removed with forceps. This type of wound leaves a bare stroma with the epithelium and basement membrane removed. 1 nmol (5.0 μL) of self-delivery siRNA resuspended in PBS was applied. In general, *in vivo* dosage ranges widely from 0.3 to 10 nmol depending on the species, area being targeted, the mode of delivery, and the response to knockdown.[88–91] Six wounded eyes were treated with NTC (Advirna), and six wounded eyes were treated with sd-USP10-targeting siRNA (US09, Advirna). According to the adherence to the Association for Research in Vision and Ophthalmology (ARVO) Statement for the Use of Animals in Ophthalmic and Vision Research, the contralateral eye served as an untouched (naive) control. E-collars were used for all wounded animals.

Slit-Lamp Biomicroscopy

After surgery, a slit lamp microscope was used to evaluate ocular health, corneal haze, and wound closure. Epithelial wound closure was assessed using fluorescein (Flucaine [5 mL], OCuSOFT, one drop per eye) and imaged on days 1, 2, 3, and 7 using a slit lamp microscope (Nikon NS-1) equipped with a digital camera with a cobalt blue filter. Images were analyzed by two independent graders for wound closure quantified by the absence of fluorescein staining over time.

Immunohistochemistry: Frozen Sections

Immediately after sacrifice, globes were enucleated and corneas were excised from globes. The cornea was cut in half through the wound and immediately submerged in a plastic mold with OCT compound (Fisher Scientific) to be frozen at −80°C. For cutting the sections, the cryostat temperature was between −20°C and −23°C, and sections were cut at 7 μm. 3–4 sections were placed per slide and stored at −80°C. Slides were thawed and baked overnight in a slide moat at 37°C. On the next day sections were rehydrated in PBS for 15 min, treated with blocking buffer (10% normal goat serum in PBS, Jackson ImmunoResearch Laboratories) for 20 min, and then incubated with primary antibodies (FN-EDA [Sigma, F6140], collagen III [Novus Biologicals, NBP105119B], α-SMA [Sigma, C6198], CD45 Thermo Fisher Scientific, MA5-28392]) at 1:250 for 1 h in a moist chamber at room temperature (RT). Slides are washed in PBS for 15 min and sections were treated with blocking buffer for 15 min. Tissue was then incubated with secondary antibody Alexa Fluor 647 (1:250) for 45 min in a moist chamber. After washing with blocking buffer for 15 min, slides were mounted with ProLong Gold antifade with DAPI (Thermo Fisher Scientific).

TUNEL Assay

All of the solutions were supplied with the kit (R&D Systems TdT *in situ* apoptosis detection kit-fluorescein, 4812-30-K). Slides were thawed and baked overnight in a slide moat at 37°C. On the next day, sections were rehydrated in PBS for 15 min, fixed in acetone (Fisher Scientific, A18500) for 10 min, at RT and washed in PBS twice for 5 min. The tissue was post-fixed in pre-cooled ethanol (UltraPure, 200CSGP)/acetic acid (Sigma, A6283, 100 mL) 2:1 for 5 min at RT,

followed by two washes in PBS. The equilibration buffer was then incubated directly on the specimen for 10 s at RT. The excess liquid was gently removed and the working strength TdT enzyme was incubated in a humid chamber at 37°C for 1 h. The working strength stop/wash buffer was then incubated for 10 min at RT. The slides were washed in three changes of PBS for 1 min each wash. The excess of liquid was removed and the working strength anti-digoxigenin conjugate was applied for 30 min at RT in a humid chamber, avoiding exposure to light. Slides were washed in PBS four times, 2 min each wash. After washing, slides were mounted with ProLong Gold antifade with DAPI (Thermo Fisher Scientific).

Quantification of Histochemistry

For collagen III, FN-EDA, CD45, and α-SMA, imaging was performed using the Nikon Eclipse Ni microscope using fixed exposure times for each antibody stain. Images were taken consecutively of the entire cornea using the ×4 objective and were then processed in ImageJ by the "apply threshold" plugin. A fixed threshold was generated using control tissue to cancel background/baseline levels of fluorescence, which was then applied to all Wnd-NTC and Wnd-US09 images, thus binarizing pixel intensity. Signal above this threshold was considered "scar," and signal below this threshold was "unscarred." For collagen III, FN-EDA, and CD45 staining, the number of pixels above threshold was then quantified in each corneal section and divided by the total number of pixels composing the scarred portion of the cornea to generate a "% pixels above threshold" metric of scarring severity. Because α-SMA staining was restricted to small and isolated pockets of cells within the corneal scar (and thus minute portions of the total area of the scar), α-SMA staining was simply reported as the total number of pixels above threshold.

Cell proliferation was determined utilizing collagen III-stained sections to mark the scar tissue. Quantification was restricted to only the scarred portion of the cornea, which was defined by an abrupt and readily observable increase in epithelial thickness as well as an abrupt increase in collagen III staining (in the anterior portion of the stroma, directly adjacent to the epithelium). "Inside the wound" corresponds to stroma with collagen III staining, whereas "outside the wound" was defined as the remaining stroma, posterior cornea beneath the scar to the endothelium. DAPI-labeled nuclei were then quantified in these portions of the stroma using the "object counter" plugin in ImageJ software. These counts were normalized by the total area of each portion to generate a nuclei density measurement.

OCT

OCT was recorded using a Bioptigen Envisu R2210 with a 10-mm telecentric lens directly prior to sacrifice. OCT datasets comprise 100 transverse sections spanning 6 mm of the eye (the central wound). Each section has a width of 6 mm (1,000 pixels) and a depth of 1.491 mm (1,024 pixels). Regions of each image containing cornea are identified using the MATLAB function "imbinarize" with the adaptive thresholding method, and all other pixels of the image are reduced to zero intensity. Corneal thickness was measured at pixel resolution in these thresholded images as the distance across the nonzero region, and thickness was averaged across the entire cornea. With regard to OCT variance, aberrations in cornea (i.e., scarring) increase nonuniformity of pixel intensities in localized areas of the cornea. To quantify this nonuniformity, we first segmented the cornea in each image file into 100 equal parts. For each segment the statistical variance (i.e., SD2) of pixel intensities was calculated. This yields 100 variances for each transverse section. Transverse sections from a dataset are averaged yielding a two-dimensional "variance by position" plot.

Statistical Analysis

Numerical data are expressed as the mean ± SEM of six animals. Statistical significance for histological analysis of three groups (UnWnd, Wnd-NTC, and Wnd-US09) was calculated by one-way ANOVA with Bonferroni's test. Statistical significance of all other numerical data was calculated with the Student's t test. *$p < 0.05$, **$p < 0.01$, ***$p < 0.001$.

SUPPLEMENTAL INFORMATION

Supplemental Information can be found online at https://doi.org/10.1016/j.omtn.2020.07.032.

AUTHOR CONTRIBUTIONS

Investigation, E.F.B., N.C., A.T.P., A.D.W., T.S., and M.R.; Methodology, E.F.B., N.C., A.D.W., T.S., S.M.M, M.R., and A.M.B.; Validation, E.F.B., N.C., M.R. and A.M.B.; Formal Analysis, E.F.B., J.E.C., T.S., M.R. and A.M.B.; Data Curation, E.F.B., N.C., and A.M.B.; Visualization, E.F.B., M.R., and A.M.B.; Resources, N.C.; Supervision, J.E.C. and A.M.B.; Writing – Review & Editing, A.D.W., T.S., and A.M.B.; Writing – Original Draft, A.M.B.; Software, M.R.; Conceptualization, A.M.B.; Project Administration, A.M.B.; Funding Acquisition, A.M.B.

CONFLICTS OF INTEREST

The authors declare no competing interests.

ACKNOWLEDGMENTS

This work was supported by NIH-NEI R01 EY024942 and R01 EY030567, SUNY Upstate Start-up Funds, an unrestricted grant to the Department of Ophthalmology & Visual Sciences from Research to Prevent Blindness, and The Lion's District 20-Y.

REFERENCES

1. Barrientez, B., Nicholas, S.E., Whelchel, A., Sharif, R., Hjortdal, J., and Karamichos, D. (2019). Corneal injury: clinical and molecular aspects. Exp. Eye Res. *186*, 107709.

2. Holló, G. (2017). Wound healing and glaucoma surgery: modulating the scarring process with conventional antimetabolites and new molecules. Dev. Ophthalmol. *59*, 80–89.

3. Morescalchi, F., Duse, S., Gambicorti, E., Romano, M.R., Costagliola, C., and Semeraro, F. (2013). Proliferative vitreoretinopathy after eye injuries: an overexpression of growth factors and cytokines leading to a retinal keloid. Mediators Inflamm. *2013*, 269787.

4. Kunikata, H., Abe, T., and Nakazawa, T. (2019). Historical, current and future approaches to surgery for rhegmatogenous retinal detachment. Tohoku J. Exp. Med. *248*, 159–168.

5. Rajan, M.S., O'Brart, D.P., Patmore, A., and Marshall, J. (2006). Cellular effects of mitomycin-C on human corneas after photorefractive keratectomy. J. Cataract Refract. Surg. *32*, 1741–1747.

6. Jester, J.V., Nien, C.J., Vasiliou, V., and Brown, D.J. (2012). Quiescent keratocytes fail to repair MMC induced DNA damage leading to the long-term inhibition of myofibroblast differentiation and wound healing. Mol. Vis. *18*, 1828–1839.

7. Rubinfeld, R.S., Pfister, R.R., Stein, R.M., Foster, C.S., Martin, N.F., Stoleru, S., Talley, A.R., and Speaker, M.G. (1992). Serious complications of topical mitomycin-C after pterygium surgery. Ophthalmology *99*, 1647–1654.

8. Safianik, B., Ben-Zion, I., and Garzozi, H.J. (2002). Serious corneoscleral complications after pterygium excision with mitomycin C. Br. J. Ophthalmol. *86*, 357–358.

9. Tandon, A., Sharma, A., Rodier, J.T., Klibanov, A.M., Rieger, F.G., and Mohan, R.R. (2013). BMP7 gene transfer via gold nanoparticles into stroma inhibits corneal fibrosis in vivo. PLoS ONE *8*, e66434.

10. Gupta, S., Rodier, J.T., Sharma, A., Giuliano, E.A., Sinha, P.R., Hesemann, N.P., Ghosh, A., and Mohan, R.R. (2017). Targeted AAV5-Smad7 gene therapy inhibits corneal scarring in vivo. PLoS ONE *12*, e0172928.

11. Gupta, S., Fink, M.K., Ghosh, A., Tripathi, R., Sinha, P.R., Sharma, A., Hesemann, N.P., Chaurasia, S.S., Giuliano, E.A., and Mohan, R.R. (2018). Novel combination *BMP7* and *HGF* gene therapy instigates selective myofibroblast apoptosis and reduces corneal haze in vivo. Invest. Ophthalmol. Vis. Sci. *59*, 1045–1057.

12. Chouhan, G., Moakes, R.J.A., Esmaeili, M., Hill, L.J., deCogan, F., Hardwicke, J., Rauz, S., Logan, A., and Grover, L.M. (2019). A self-healing hydrogel eye drop for the sustained delivery of decorin to prevent corneal scarring. Biomaterials *210*, 41–50.

13. Hill, L.J., Moakes, R.J.A., Vareechon, C., Butt, G., Ng, A., Brock, K., Chouhan, G., Vincent, R.C., Abbondante, S., Williams, R.L., et al. (2018). Sustained release of decorin to the surface of the eye enables scarless corneal regeneration. NPJ Regen. Med. *3*, 23.

14. Shojaati, G., Khandaker, I., Funderburgh, M.L., Mann, M.M., Basu, R., Stolz, D.B., Geary, M.L., Dos Santos, A., Deng, S.X., and Funderburgh, J.L. (2019). Mesenchymal stem cells reduce corneal fibrosis and inflammation via extracellular vesicle-mediated delivery of miRNA. Stem Cells Transl. Med. *8*, 1192–1201.

15. Stern, J.H., Tian, Y., Funderburgh, J., Pellegrini, G., Zhang, K., Goldberg, J.L., Ali, R.R., Young, M., Xie, Y., and Temple, S. (2018). Regenerating eye tissues to preserve and restore vision. cell stem cell *22*, 834–849.

16. Fernández-Pérez, J., and Ahearne, M. (2020). Decellularization and recellularization of cornea: progress towards a donor alternative. Methods *171*, 86–96.

17. Ritchey, E.R., Code, K., Zelinka, C.P., Scott, M.A., and Fischer, A.J. (2011). The chicken cornea as a model of wound healing and neuronal re-innervation. Mol. Vis. *17*, 2440–2454.

18. DelMonte, D.W., and Kim, T. (2011). Anatomy and physiology of the cornea. J. Cataract Refract. Surg. *37*, 588–598.

19. Marino, G.K., Santhiago, M.R., Santhanam, A., Lassance, L., Thangavadivel, S., Medeiros, C.S., Bose, K., Tam, K.P., and Wilson, S.E. (2017). Epithelial basement membrane injury and regeneration modulates corneal fibrosis after pseudomonas corneal ulcers in rabbits. Exp. Eye Res. *161*, 101–105.

20. Wilson, S.E., Marino, G.K., Torricelli, A.A.M., and Medeiros, C.S. (2017). Injury and defective regeneration of the epithelial basement membrane in corneal fibrosis: a paradigm for fibrosis in other organs? Matrix Biol. *64*, 17–26.

21. Saikia, P., Medeiros, C.S., Thangavadivel, S., and Wilson, S.E. (2018). Basement membranes in the cornea and other organs that commonly develop fibrosis. Cell Tissue Res. *374*, 439–453.

22. Stepp, M.A., Zieske, J.D., Trinkaus-Randall, V., Kyne, B.M., Pal-Ghosh, S., Tadvalkar, G., and Pajoohesh-Ganji, A. (2014). Wounding the cornea to learn how it heals. Exp. Eye Res. *121*, 178–193.

23. Hinz, B. (2007). Formation and function of the myofibroblast during tissue repair. J. Invest. Dermatol. *127*, 526–537.

24. Coentro, J.Q., Pugliese, E., Hanley, G., Raghunath, M., and Zeugolis, D.I. (2019). Current and upcoming therapies to modulate skin scarring and fibrosis. Adv. Drug Deliv. Rev. *146*, 37–59.

25. Horowitz, J.C., and Thannickal, V.J. (2019). Mechanisms for the resolution of organ fibrosis. Physiology (Bethesda) *34*, 43–55.

26. Black, L.M., Lever, J.M., and Agarwal, A. (2019). Renal inflammation and fibrosis: a double-edged sword. J. Histochem. Cytochem. *67*, 663–681.

27. Parola, M., and Pinzani, M. (2019). Liver fibrosis: pathophysiology, pathogenetic targets and clinical issues. Mol. Aspects Med. *65*, 37–55.

28. Gillespie, S.R., Tedesco, L.J., Wang, L., and Bernstein, A.M. (2017). The deubiquitylase USP10 regulates integrin β1 and β5 and fibrotic wound healing. J. Cell Sci. *130*, 3481–3495.

29. Wang, L., Pedroja, B.S., Meyers, E.E., Garcia, A.L., Twining, S.S., and Bernstein, A.M. (2012). Degradation of internalized αvβ5 integrin is controlled by uPAR bound uPA: effect on β1 integrin activity and α-SMA stress fiber assembly. PLoS ONE *7*, e33915.

30. Leask, A. (2013). Integrin β1: a mechanosignaling sensor essential for connective tissue deposition by fibroblasts. Adv. Wound Care (New Rochelle) *2*, 160–166.

31. Henderson, N.C., and Sheppard, D. (2013). Integrin-mediated regulation of TGFβ in fibrosis. Biochim. Biophys. Acta *1832*, 891–896.

32. Reed, N.I., Jo, H., Chen, C., Tsujino, K., Arnold, T.D., DeGrado, W.F., and Sheppard, D. (2015). The $\alpha_v\beta_1$ integrin plays a critical in vivo role in tissue fibrosis. Sci. Transl. Med. *7*, 288ra79.

33. Henderson, N.C., Arnold, T.D., Katamura, Y., Giacomini, M.M., Rodriguez, J.D., McCarty, J.H., Pellicoro, A., Raschperger, E., Betsholtz, C., Ruminski, P.G., et al. (2013). Targeting of α_v integrin identifies a core molecular pathway that regulates fibrosis in several organs. Nat. Med. *19*, 1617–1624.

34. Mamuya, F.A., Wang, Y., Roop, V.H., Scheiblin, D.A., Zajac, J.C., and Duncan, M.K. (2014). The roles of α_V integrins in lens EMT and posterior capsular opacification. J. Cell. Mol. Med. *18*, 656–670.

35. Hinz, B. (2015). The extracellular matrix and transforming growth factor-β1: tale of a strained relationship. Matrix Biol. *47*, 54–65.

36. Wipff, P.J., Rifkin, D.B., Meister, J.J., and Hinz, B. (2007). Myofibroblast contraction activates latent TGF-β1 from the extracellular matrix. J. Cell Biol. *179*, 1311–1323.

37. Wipff, P.J., and Hinz, B. (2008). Integrins and the activation of latent transforming growth factor β1—an intimate relationship. Eur. J. Cell Biol. *87*, 601–615.

38. Walraven, M., and Hinz, B. (2018). Therapeutic approaches to control tissue repair and fibrosis: extracellular matrix as a game changer. Matrix Biol. *71–72*, 205–224.

39. Lobert, V.H., and Stenmark, H. (2010). Ubiquitination of α-integrin cytoplasmic tails. Commun. Integr. Biol. *3*, 583–585.

40. Hsia, H.C., Nair, M.R., and Corbett, S.A. (2014). The fate of internalized α5 integrin is regulated by matrix-capable fibronectin. J. Surg. Res. *191*, 268–279.

41. Castro, N., Gillespie, S.R., and Bernstein, A.M. (2019). Ex vivo corneal organ culture model for wound healing studies. J. Vis. Exp. (144).

42. Yuan, J., Luo, K., Zhang, L., Cheville, J.C., and Lou, Z. (2010). USP10 regulates p53 localization and stability by deubiquitinating p53. Cell *140*, 384–396.

43. Guzman-Aranguez, A., Loma, P., and Pintor, J. (2013). Small-interfering RNAs (siRNAs) as a promising tool for ocular therapy. Br. J. Pharmacol. *170*, 730–747.

44. Jiang, J., Zhang, X., Tang, Y., Li, S., and Chen, J. (2020). Progress on ocular siRNA gene-silencing therapy and drug delivery systems. Fundam. Clin. Pharmacol. Published online April 16, 2020. https://doi.org/10.1111/fcp.12561.

45. Khvorova, A., and Watts, J.K. (2017). The chemical evolution of oligonucleotide therapies of clinical utility. Nat. Biotechnol. *35*, 238–248.

46. Alterman, J.F., Hall, L.M., Coles, A.H., Hassler, M.R., Didiot, M.C., Chase, K., Abraham, J., Sottosanti, E., Johnson, E., Sapp, E., et al. (2015). Hydrophobically modified siRNAs silence huntingtin mRNA in primary neurons and mouse brain. Mol. Ther. Nucleic Acids *4*, e266.

47. Byrne, M., Tzekov, R., Wang, Y., Rodgers, A., Cardia, J., Ford, G., Holton, K., Pandarinathan, L., Lapierre, J., Stanney, W., et al. (2013). Novel hydrophobically modified asymmetric RNAi compounds (sd-rxRNA) demonstrate robust efficacy in the eye. J. Ocul. Pharmacol. Ther. *29*, 855–864.

48. Hassler, M.R., Turanov, A.A., Alterman, J.F., Haraszti, R.A., Coles, A.H., Osborn, M.F., Echeverria, D., Nikan, M., Salomon, W.E., Roux, L., et al. (2018). Comparison of partially and fully chemically-modified siRNA in conjugate-mediated delivery in vivo. Nucleic Acids Res. *46*, 2185–2196.

49. Shmushkovich, T., Monopoli, K.R., Homsy, D., Leyfer, D., Betancur-Boissel, M., Khvorova, A., and Wolfson, A.D. (2018). Functional features defining the efficacy of cholesterol-conjugated, self-deliverable, chemically modified siRNAs. Nucleic Acids Res. *46*, 10905–10916.

50. Haraszti, R.A., Roux, L., Coles, A.H., Turanov, A.A., Alterman, J.F., Echeverria, D., Godinho, B.M.D.C., Aronin, N., and Khvorova, A. (2017). 5'-Vinylphosphonate improves tissue accumulation and efficacy of conjugated siRNAs in vivo. Nucleic Acids Res. *45*, 7581–7592.

51. Chan, T., Payor, S., and Holden, B.A. (1983). Corneal thickness profiles in rabbits using an ultrasonic pachometer. Invest. Ophthalmol. Vis. Sci. *24*, 1408–1410.

52. Karamichos, D., Guo, X.Q., Hutcheon, A.E., and Zieske, J.D. (2010). Human corneal fibrosis: an in vitro model. Invest. Ophthalmol. Vis. Sci. *51*, 1382–1388.

53. Lorenzo-Martín, E., Gallego-Muñoz, P., Mar, S., Fernández, I., Cidad, P., and Martínez-García, M.C. (2019). Dynamic changes of the extracellular matrix during corneal wound healing. Exp. Eye Res. *186*, 107704.

54. Wilson, S.E., He, Y.G., Weng, J., Li, Q., McDowall, A.W., Vital, M., and Chwang, E.L. (1996). Epithelial injury induces keratocyte apoptosis: hypothesized role for the interleukin-1 system in the modulation of corneal tissue organization and wound healing. Exp. Eye Res. *62*, 325–327.

55. Kaur, H., Chaurasia, S.S., Agrawal, V., Suto, C., and Wilson, S.E. (2009). Corneal myofibroblast viability: opposing effects of IL-1 and TGF β1. Exp. Eye Res. *89*, 152–158.

56. Ossowski, L., and Aguirre-Ghiso, J.A. (2000). Urokinase receptor and integrin partnership: coordination of signaling for cell adhesion, migration and growth. Curr. Opin. Cell Biol. *12*, 613–620.

57. Kanno, Y., Kaneiwa, A., Minamida, M., Kanno, M., Tomogane, K., Takeuchi, K., Okada, K., Ueshima, S., Matsuo, O., and Matsuno, H. (2008). The absence of uPAR is associated with the progression of dermal fibrosis. J. Invest. Dermatol. *128*, 2792–2797.

58. Manetti, M., Rosa, I., Milia, A.F., Guiducci, S., Carmeliet, P., Ibba-Manneschi, L., and Matucci-Cerinic, M. (2014). Inactivation of urokinase-type plasminogen activator receptor (uPAR) gene induces dermal and pulmonary fibrosis and peripheral microvasculopathy in mice: a new model of experimental scleroderma? Ann. Rheum. Dis. *73*, 1700–1709.

59. Manetti, M., Rosa, I., Fazi, M., Guiducci, S., Carmeliet, P., Ibba-Manneschi, L., and Matucci-Cerinic, M. (2016). Systemic sclerosis-like histopathological features in the myocardium of uPAR-deficient mice. Ann. Rheum. Dis. *75*, 474–478.

60. Li, Z., Burns, A.R., and Smith, C.W. (2006). Two waves of neutrophil emigration in response to corneal epithelial abrasion: distinct adhesion molecule requirements. Invest. Ophthalmol. Vis. Sci. *47*, 1947–1955.

61. Sahu, S.K., Mittal, S.K., Foulsham, W., Li, M., Sangwan, V.S., and Chauhan, S.K. (2018). Mast cells initiate the recruitment of neutrophils following ocular surface injury. Invest. Ophthalmol. Vis. Sci. *59*, 1732–1740.

62. Bratton, D.L., and Henson, P.M. (2011). Neutrophil clearance: when the party is over, clean-up begins. Trends Immunol. *32*, 350–357.

63. Lassance, L., Marino, G.K., Medeiros, C.S., Thangavadivel, S., and Wilson, S.E. (2018). Fibrocyte migration, differentiation and apoptosis during the corneal wound healing response to injury. Exp. Eye Res. *170*, 177–187.

64. Takayama, K.I., Suzuki, T., Fujimura, T., Takahashi, S., and Inoue, S. (2018). Association of USP10 with G3BP2 inhibits p53 signaling and contributes to poor outcome in prostate cancer. Mol. Cancer Res. *16*, 846–856.

65. Zhang, H., Zhang, S.H., He, H.W., Zhang, C.X., Yu, D.K., and Shao, R.G. (2013). Downregulation of G3BPs inhibits the growth, migration and invasion of human lung carcinoma H1299 cells by suppressing the Src/FAK-associated signaling pathway. Cancer Gene Ther. *20*, 622–629.

66. Deng, C.C., Zhu, D.H., Chen, Y.J., Huang, T.Y., Peng, Y., Liu, S.Y., Lu, P., Xue, Y.-H., Xu, Y.-P., Yang, B., and Rong, Z. (2019). TRAF4 promotes fibroblast proliferation in keloids by destabilizing p53 via interacting with the deubiquitinase USP10. J. Invest. Dermatol. *139*, 1925–1935.e5.

67. Hertsenberg, A.J., Shojaati, G., Funderburgh, M.L., Mann, M.M., Du, Y., and Funderburgh, J.L. (2017). Corneal stromal stem cells reduce corneal scarring by mediating neutrophil infiltration after wounding. PLoS ONE *12*, e0171712.

68. Laskin, D.L., Malaviya, R., and Laskin, J.D. (2019). Role of macrophages in acute lung injury and chronic fibrosis induced by pulmonary toxicants. Toxicol. Sci. *168*, 287–301.

69. Kitano, A., Okada, Y., Yamanka, O., Shirai, K., Mohan, R.R., and Saika, S. (2010). Therapeutic potential of trichostatin A to control inflammatory and fibrogenic disorders of the ocular surface. Mol. Vis. *16*, 2964–2973.

70. Wilson, C.L., Murphy, L.B., Leslie, J., Kendrick, S., French, J., Fox, C.R., Sheerin, N.S., Fisher, A., Robinson, J.H., Tiniakos, D.G., et al. (2015). Ubiquitin C-terminal hydrolase 1: a novel functional marker for liver myofibroblasts and a therapeutic target in chronic liver disease. J. Hepatol. *63*, 1421–1428.

71. Soji, K., Doi, S., Nakashima, A., Sasaki, K., Doi, T., and Masaki, T. (2018). Deubiquitinase inhibitor PR-619 reduces Smad4 expression and suppresses renal fibrosis in mice with unilateral ureteral obstruction. PLoS ONE *13*, e0202409.

72. Neves-Carvalho, A., Logarinho, E., Freitas, A., Duarte-Silva, S., Costa, Mdo.C., Silva-Fernandes, A., Martins, M., Serra, S.C., Lopes, A.T., Paulson, H.L., et al. (2015). Dominant negative effect of polyglutamine expansion perturbs normal function of ataxin-3 in neuronal cells. Hum. Mol. Genet. *24*, 100–117.

73. do Carmo Costa, M., Bajanca, F., Rodrigues, A.J., Tomé, R.J., Corthals, G., Macedo-Ribeiro, S., Paulson, H.L., Logarinho, E., and Maciel, P. (2010). Ataxin-3 plays a role in mouse myogenic differentiation through regulation of integrin subunit levels. PLoS ONE *5*, e11728.

74. Harrigan, J.A., Jacq, X., Martin, N.M., and Jackson, S.P. (2018). Deubiquitylating enzymes and drug discovery: emerging opportunities. Nat. Rev. Drug Discov. *17*, 57–78.

75. Poondla, N., Chandrasekaran, A.P., Kim, K.S., and Ramakrishna, S. (2019). Deubiquitinating enzymes as cancer biomarkers: new therapeutic opportunities? BMB Rep. *52*, 181–189.

76. Zhang, W., Bailey-Elkin, B.A., Knaap, R.C.M., Khare, B., Dalebout, T.J., Johnson, G.G., van Kasteren, P.B., McLeish, N.J., Gu, J., He, W., et al. (2017). Potent and selective inhibition of pathogenic viruses by engineered ubiquitin variants. PLoS Pathog. *13*, e1006372.

77. Titze-de-Almeida, R., David, C., and Titze-de-Almeida, S.S. (2017). The race of 10 synthetic RNAi-based drugs to the pharmaceutical market. Pharm. Res. *34*, 1339–1363.

78. Solano, E.C., Kornbrust, D.J., Beaudry, A., Foy, J.W., Schneider, D.J., and Thompson, J.D. (2014). Toxicological and pharmacokinetic properties of QPI-1007, a chemically modified synthetic siRNA targeting caspase 2 mRNA, following intravitreal injection. Nucleic Acid Ther. *24*, 258–266.

79. Moreno-Montañés, J., Bleau, A.M., and Jimenez, A.I. (2018). Tivanisiran, a novel siRNA for the treatment of dry eye disease. Expert Opin. Investig. Drugs *27*, 421–426.

80. Benitez-Del-Castillo, J.M., Moreno-Montañés, J., Jiménez-Alfaro, I., Muñoz-Negrete, F.J., Turman, K., Palumaa, K., Sádaba, B., González, M.V., Ruz, V., Vargas, B., et al. (2016). Safety and efficacy clinical trials for SYL1001, a novel short interfering RNA for the treatment of dry eye disease. Invest. Ophthalmol. Vis. Sci. *57*, 6447–6454.

81. Solinís, M.A., del Pozo-Rodríguez, A., Apaolaza, P.S., and Rodríguez-Gascón, A. (2015). Treatment of ocular disorders by gene therapy. Eur. J. Pharm. Biopharm. *95* (Pt B), 331–342.

82. Watts, J.K., Brown, R.H., and Khvorova, A. (2019). Nucleic acid therapeutics for neurological diseases. Neurotherapeutics *16*, 245–247.

83. Tagalakis, A.D., Madaan, S., Larsen, S.D., Neubig, R.R., Khaw, P.T., Rodrigues, I., Goyal, S., Lim, K.S., and Yu-Wai-Man, C. (2018). In vitro and in vivo delivery of a sustained release nanocarrier-based formulation of an MRTF/SRF inhibitor in conjunctival fibrosis. J. Nanobiotechnology *16*, 97.

84. Fernando, O., Tagalakis, A.D., Awwad, S., Brocchini, S., Khaw, P.T., Hart, S.L., and Yu-Wai-Man, C. (2018). Development of targeted siRNA nanocomplexes to prevent fibrosis in experimental glaucoma filtration surgery. Mol. Ther. *26*, 2812–2822.

85. Didiot, M.C., Ferguson, C.M., Ly, S., Coles, A.H., Smith, A.O., Bicknell, A.A., Hall, L.M., Sapp, E., Echeverria, D., Pai, A.A., et al. (2018). Nuclear localization of huntingtin mRNA is specific to cells of neuronal origin. Cell Rep *24*, 2553–2560.e5.

86. Bernstein, A.M., Greenberg, R.S., Taliana, L., and Masur, S.K. (2004). Urokinase anchors uPAR to the actin cytoskeleton. Invest. Ophthalmol. Vis. Sci. *45*, 2967–2977.

87. Tripathi, R., Giuliano, E.A., Gafen, H.B., Gupta, S., Martin, L.M., Sinha, P.R., Rodier, J.T., Fink, M.K., Hesemann, N.P., Chaurasia, S.S., and Mohan, R.R. (2019). Is sex a biological variable in corneal wound healing? Exp. Eye Res. *187*, 107705.

88. Xu, H., Rösler, T.W., Carlsson, T., de Andrade, A., Fiala, O., Hollerhage, M., Oertel, W.H., Goedert, M., Aigner, A., and Höglinger, G.U. (2014). Tau silencing by siRNA in the P301S mouse model of tauopathy. Curr. Gene Ther. *14*, 343–351.

89. Loma, P., Guzman-Aranguez, A., Pérez de Lara, M.J., and Pintor, J. (2015). Diadenosine tetraphosphate induces tight junction disassembly thus increasing corneal epithelial permeability. Br. J. Pharmacol. *172*, 1045–1058.

90. Hegde, V., Hickerson, R.P., Nainamalai, S., Campbell, P.A., Smith, F.J., McLean, W.H., and Pedrioli, D.M. (2014). In vivo gene silencing following non-invasive siRNA delivery into the skin using a novel topical formulation. J. Control. Release *196*, 355–362.

91. Schiroli, D., Gómara, M.J., Maurizi, E., Atkinson, S.D., Mairs, L., Christie, K.A., Cobice, D.F., McCrudden, C.M., Nesbit, M.A., Haro, I., and Moore, T. (2019). Effective in vivo topical delivery of siRNA and gene silencing in intact corneal epithelium using a modified cell-penetrating peptide. Mol. Ther. Nucleic Acids *17*, 891–906.

92. Takahashi, M., Higuchi, M., Matsuki, H., Yoshita, M., Ohsawa, T., Oie, M., and Fujii, M. (2013). Stress granules inhibit apoptosis by reducing reactive oxygen species production. Mol. Cell. Biol. *33*, 815–829.